

Imperceptible Adversarial Examples in the Physical World

Weilin Xu¹, Sebastian Szyller¹, Cory Cornelius¹, Luis Murillo Rojas¹, Marius Arvinte¹, Alvaro Velasquez², Jason Martin^{* 3}, and Nageen Himayat¹

¹Intel

²University of Colorado Boulder

³HiddenLayer

Abstract

Adversarial examples in the digital domain against deep learning-based computer vision models allow for perturbations that are imperceptible to human eyes. However, producing similar adversarial examples in the physical world has been difficult due to the non-differentiable image distortion functions in visual sensing systems. The existing algorithms for generating physically realizable adversarial examples often loosen their definition of adversarial examples by allowing unbounded perturbations, resulting in obvious or even strange visual patterns. In this work, we make adversarial examples imperceptible in the physical world using a straight-through estimator (STE, a.k.a. BPDA). We employ STE to overcome the non-differentiability – applying exact, non-differentiable distortions in the forward pass of the backpropagation step, and using the identity function in the backward pass. Our differentiable rendering extension to STE also enables imperceptible adversarial patches in the physical world. Using printout photos, and experiments in the CARLA simulator, we show that STE enables fast generation of ℓ_∞ bounded adversarial examples despite the non-differentiable distortions. To the best of our knowledge, this is the first work demonstrating imperceptible adversarial examples bounded by small ℓ_∞ norms in the physical world that force zero classification accuracy in the global perturbation threat model and cause near-zero (4.22%) AP50 in object detection in the patch perturbation threat model. We urge the community to re-evaluate the threat of adversarial examples in the physical world.

1. Introduction

Deep Neural Networks (DNNs) have been the *de facto* solutions to many computer vision problems thanks to their ex-

ceptional accuracy compared with previous methods. However, DNNs are susceptible to *adversarial examples* that degrade performance down to near-zero on most tasks. It is easy to generate adversarial examples against any DNNs using attacks based on gradient descent and backpropagation – such as *Fast Gradient Sign Method* (FGSM) [35] or Projected Gradient Descent (PGD) [27]. On the contrary, attacking visual sensing systems in the physical world is more difficult due to the non-differentiable distortion functions in the imaging pipeline.

Prior work on physically realizable adversarial examples loosen the definition of adversarial examples by allowing unbounded perturbations confined to a portion of the image [2, 11, 21]. This increases the chance of the perturbations surviving the non-differentiable distortions in the target system. However, as a side-effect it can lead to obvious or even strange textures in the generated perturbations, making them easier to spot [6, 11, 40]. As a result, adversarial examples do not deter practitioners from deploying DNNs in security-sensitive scenarios, such as video surveillance systems [31] and autonomous vehicles [17]. Black Hat Briefings has been reluctant to accept submissions on adversarial examples against visual sensing systems in its AI track, as “industry hasn’t cared much because it doesn’t impact most of them” [20].

In this work, we challenge the belief that adversarial examples are not a threat thanks to the image distortions in a visual sensing system serving as an effective defense. Our work focuses on *imperceptible* perturbations in the physical domain that are aligned with the original definition [35]. We demonstrate that physically realizable adversarial examples are achievable and a real threat that requires serious consideration. Hence, practitioners should re-evaluate the security implications of *Deep Neural Network* (DNN)-based visual sensing systems and assume that adversarial examples in the physical world can be as effective as in the digital domain.

In this work, we develop a novel approach based on

^{*}Contributed to the work while at Intel.






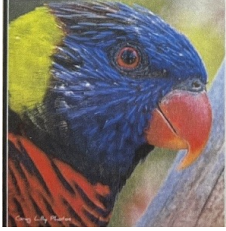
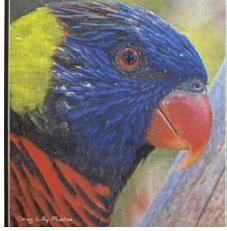



	Benign	$\epsilon = 2/255$	$\epsilon = 4/255$	$\epsilon = 8/255$	$\epsilon = 16/255$
Digital Image					
Printed Image					
ResNet-50 Prediction	Lorikeet 99.26%	Coucal 80.91%	Coucal 99.98%	Coucal 100.00%	Coucal 100.00%

Figure 1. Straight-through estimator (STE, a.k.a. BPDA) combined with PGD reliably produces imperceptible adversarial examples in the physical world that fool the target model – a pre-trained ResNet50 image classifier. We consider global adversarial perturbations bounded by $\ell_\infty = 2|4|8|16$. See experimental details in Section 3.

Straight-through Estimator (STE) to generate adversarial examples against DNN-based visual sensing systems that distort images with non-differentiable functions, such as inaccurate colors in printers, clipping of electrical signals caused by photodiodes or power amplifiers [7]. Our key insight is that we overcome such distortions using non-differentiable components in the forward pass without any approximation, and using the identity function or differentiable rendering in the backward pass to enable backpropagation. In experiments with the paper printouts and the CARLA simulator, we show that our attack in the physical world has comparable effectiveness to classic attacks in the digital domain. Additionally, our method can generate ℓ_∞ bounded adversarial examples with imperceptible perturbations that are effective in the physical world (as shown in Figure 1).

1.1. Contributions

We claim the following contributions:

1. We propose a novel attack that uses STE and differentiable rendering to generate adversarial examples against DNN-based visual sensing systems that contain non-differentiable distortion functions in their imaging pipelines (Section 3.1 and Section 4.1).
2. We demonstrate how to use STE in the global perturbation threat model to produce imperceptible adversarial examples bounded by $\ell_\infty = 4/255$ on paper printouts that force *zero* accuracy on the target model (Section 3).
3. We combine STE with differentiable rendering to pro-

duce imperceptible adversarial patches in the CARLA urban driving simulator [18] which is built upon *Unreal Engine 4* (UE4) [19] with a non-differentiable 3D renderer. We show that our method produces unbounded adversarial patches that lower AP50 of object detection from 43.29% to 0% and imperceptible adversarial patches bounded by $\ell_\infty = \frac{8}{255}$ that decrease AP50 from 43.29% to 4.22% (Section 4).

2. Background & Related Work

Adversarial examples. Despite substantial research, present-day neural networks remain susceptible to adversarial examples [1, 9, 10], with no computationally efficient defense being widely adopted. Defenses that have empirical success [27], or theoretical performance guarantees [12] typically increase the cost of training or inference by at least one order of magnitude. An adversary crafts an adversarial example by adding an imperceptible, crafted perturbation to a test sample, and uses it to conduct a *model evasion* attack that fools the model into making a wrong prediction. This is formalized as solving the following constrained optimization problem:

$$\underset{\delta}{\operatorname{argmin}} \mathcal{L}(f(x + \delta), y_{\text{target}}), \quad \text{s.t. } \delta \in \mathcal{S}, \quad (1)$$

where f is the end-to-end processing that produces the estimated output obtained from perturbing the input x with δ , y_{target} is the desired output, \mathcal{L} is the loss function minimized by the adversary, and \mathcal{S} is a constraint set placed on

the perturbation δ .

Generating ℓ_p bounded adversarial examples with an imperceptible perturbation in the digital domain using gradient-based approaches is trivial. However, similar adversarial examples are less effective in the physical space – if they are printed out, or a camera is used to capture them and feed the frames to the target model [24]. This is due to the fact that visual sensing systems distort images by passing them through complex processing pipelines [7, 28] that many attack algorithms do not take into account.

A straightforward way to overcome this is to accurately model the distortion function of the printer (or the screen) and the camera using a differentiable function. However, this requires non-trivial effort and is usually infeasible, given the complicated modern image capture pipelines [3].

Approaches that attempt to overcome the non-differentiability in generating adversarial examples in the physical world can be divided into three groups: perturbation constraints, *Expectation over Transformation* (EoT), and neural rendering. Recent work on physically realizable adversarial examples often combines techniques from multiple categories [34, 42].

Perturbation constraints. Printers and screens do not produce colors with 100% accuracy [3]. Furthermore, imaging sensors do not capture pixels perfectly. To account for the limitations of rendering and imaging pipelines, and produce effective adversarial examples, we need to lower the discrepancy between a digital image and its corresponding (captured) camera frame. Early work on physically realizable adversarial examples [32] proposed several physical constraints on adversarial examples: allowing limited printable colors, encouraging smooth textures with the total variance term, and using manual color management to calibrate the printing colors. Such physical constraints enable adversarial eyeglasses frames that fool a face recognition system. **EoT.** Although modeling the exact distortion functions in the non-differentiable components is non-trivial, we can make adversarial examples robust to distortions in the digital domain. Hence, the robustness to simulated distortions may generalize well to the actual distortions in the target visual sensing system. Athalye et al. proposed EoT to approximate unknown distortion functions with random image transformations, including rescaling, rotation, lightening, darkening, Gaussian noising, and translation etc [2]. EoT was later adapted to attacking object detection models in the ShapeShifter work [11].

Neural rendering. Deep neural networks can be used to approximate the non-differentiable distortion functions. Jan et al. proposed an image-to-image model that simulates the distortions of an imaging pipeline that consists of a printer and a camera [21].

Nevertheless, all these approaches increase the adversarial perturbation budget. Hence, it becomes difficult to gen-

erate ℓ_p bounded adversarial examples with imperceptible perturbations in the physical world. Many attack algorithms loosen the conventional ℓ_p constraint on pixel values in favor of unbounded perturbations. As a result, existing adversarial examples that are effective in the physical world often contain obvious or even strange visual patterns, which leads to many defense solutions dedicated to detecting such abnormal textures [22, 25].

3. Imperceptible global perturbations

In this section, we first explain how to use STE to overcome the obstacle of non-differentiable distortions in the imaging pipeline. Then, we empirically show (using paper printouts) that STE is effective in producing imperceptible adversarial examples in the physical world under the global perturbation threat model.

3.1. STE for non-differentiable distortions

We formalize a visual sensing system as follows: given a target model $f(\cdot)$, an adversary can add an ℓ_∞ -bounded perturbation δ to an image x in the digital domain. The adversary must use some device, such as a printer, to render the digital image $x + \delta$ in the physical world. The visual sensing system takes a photo of the rendered image, extracts the image and feeds it to the target model. If we model the distortions on the digital image $x + \delta$ throughout the printer-camera-extractor pipeline as $d(\cdot)$, the end-to-end visual sensing system can be expressed as:

$$y = f(d(x + \delta)), \quad (2)$$

where y is the final predicted output.

The adversary intends to influence y by finding an imperceptible perturbation δ . If $d(\cdot)$ is continuous and differentiable, generating adversarial examples against the system should be as easy as an attack in the digital domain. However, the camera is a non-differentiable function that distorts captured frames due to the imperfections of the sensor and the lens. The function of the printing device is not differentiable either, and it distorts $x + \delta$ by outputting inaccurate pixel values. Thus, the adversary can not backpropagate through $d(\cdot)$ to get the gradient of δ needed to generate adversarial examples.

A straightforward solution is to implement $d(\cdot)$ in a fully differentiable manner. But it is usually deemed too expensive or even infeasible [23].

Instead, we use STE [4] to model the non-differentiable distortions, as shown in Figure 2. STE uses the non-differentiable output in the forward pass to obtain the exact loss function value but the identity function in the backward pass to approximate its gradient with respect to the input. If the non-differentiable distortions lead to a similar image, like what a printer or a camera does, the approximation error should be small. Intuitively, if we brighten one pixel in

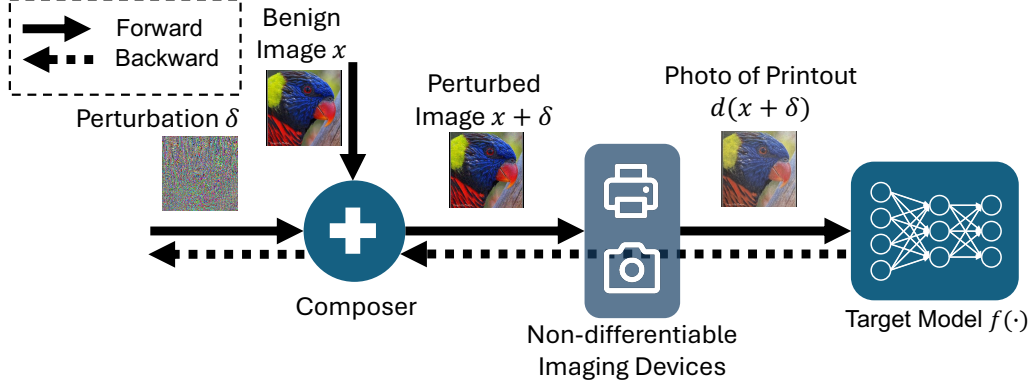


Figure 2. We use STE (a.k.a. BPDA) to cross the non-differentiable barrier of the imaging pipeline under the global perturbation threat model. The key is to calculate the accurate loss function value with the non-differentiable distortion functions in the forward pass, but use the identity function in the backward pass to estimate the gradient.

the digital image, the printer and the camera would brighten the corresponding pixel in the photo too. Thus, the sign of the approximate gradient is always accurate, even though the magnitude deviates. Coincidentally, many ℓ_∞ attack algorithms, such as FGSM and PGD, only use the gradient sign during the optimization. Therefore, STE is the optimal method to overcome non-differentiable distortions for those gradient-sign based attacks.

We use the stop-gradient ($\text{sg}[\cdot]$) operation in automatic differentiation systems to construct a differentiable imaging pipeline with distortions as:

$$\begin{aligned} f(d(x + \delta)) &= f((x + \delta) + \text{sg}[d(x + \delta) - (x + \delta)]) \\ &= f(x + \delta + C) \end{aligned} \quad (3)$$

, where C is a constant of the difference between the distorted image and the digital one.

The method is also known as *Backward Pass Differentiable Approximation* (BPDA) in the adversarial machine learning literature, and was used to break many defenses relying on non-differentiable filtering functions in the digital domain [1]. In the next sections, we show that STE allows us to overcome non-differentiable image distortions when generating adversarial examples in the physical world.

3.2. Experimental Setup

We follow the experiment by Kurakin et al. [24] to validate the power of STE in producing imperceptible adversarial examples in the physical world. We make printouts of six square images with a printer, take photos and crop out the square images to feed the target model, Figure 3.

Dataset: We randomly draw six images of different categories whose edges are not shorter than 300 pixels from the ImageNet ILSVRC validation set [16]. We make a center crop of 300×300 for all images, as shown in Figure 3.



Figure 3. We follow the experiments by Kurakin et al. [24] to validate the power of STE in producing imperceptible adversarial examples in the physical world: 1. generate a digital printout of six square images; 2. print it out and take a photo of the paper; 3. perform perspective transformation and crop out the square images that are being fed to the target model.

Target model: We use the ResNet-50 model from torchvision that is trained on the ImageNet ILSVRC dataset.

Attack algorithms: We use both the single-step FGSM and the 12-step PGD with the step size $1/255$. Both are untargeted attacks trying to increase the cross entropy loss. We consider ℓ_∞ bounds of 2, 4, 8 and 16 out of 255, which usually produce imperceptible perturbations in the physical world. We understand that they are by no means the optimal attack algorithms, but they are sufficient to force misclassifications in our experiment. We compare the performance of all attacks with and without STE.

Printout: As is shown in Figure 3, we use ArUco markers [38] and QR codes to automate the extraction of images from photos with perspective transformation and cropping. We make a total of 113 printouts in the experiment ¹.

Printer: We use a Canon imageCLASS MF642Cdw color laser printer with resolution 600x600 dpi to make all print-

¹113 = 1 benign + 4 epsilons * 2 modes * (1 PGD random init + 12 PGD iters + 1 FGSM iter)

Table 1. A comparison of FGSM and PGD attacks with and without STE in generating imperceptible adversarial examples in the physical world (the printer-camera-extractor pipeline in Figure 3). The goal of the untargeted adversary is to lower the number of correct predictions. The pure digital FGSM and PGD attacks without STE generate perturbations that are destroyed by the printing distortions, resulting in images being correctly classified in the physical world. STE consistently helps FGSM and PGD generate effective adversarial examples in the physical world, leading to zero accuracy in many cases. STE-augmented attacks perform poorly in the digital domain because the attacks compute the loss function with the physical world predictions (Equation (3)).

Method	ϵ	STE	Correct Predictions↓	
			Digital	Physical
FGSM	Benign	0	-	5/6
	2	✗	1/6	4/6
		✓	4/6	4/6
	4	✗	1/6	3/6
		✓	3/6	2/6
	8	✗	0/6	3/6
		✓	3/6	1/6
	16	✗	2/6	2/6
		✓	2/6	0/6
	PGD	2	✗	0/6
			✓	2/6
		4	✗	0/6
			✓	0/6
		8	✗	0/6
			✓	0/6
		16	✗	0/6
			✓	0/6

outs. Since it is not a photo-grade printer, we expect to see inaccurate colors and other defects in the printouts. In fact, the printing distortion is the major obstacle to generating adversarial examples.

Camera: We use the 12MP Wide Camera in an iPhone 13 Pro to take 113 photos of printouts manually. The handheld operation does not guarantee exactly the same perspective for each photo, which adds more difficulty to the adversary in modeling the distortions.

3.3. Results

We present the classification performance of the target model on the six images under various attacks in Table 1. Firstly, the image distortions in the physical world do not affect the classification performance on benign images – the same five images out of six are correctly classified. How-

ever, the same distortions destroy the digital adversarial examples as shown in prior work [24]. When we print the digital adversarial examples out on paper, the number of correct predictions increases. The target model is able to make 2/6 correct predictions with the strongest digital attack bounded by $\epsilon = 16/255$.

In contrast, we learn from the highlighted numbers in the “Physical” column of Table 1 that STE strengthens all attacks in the physical world except for FGSM bounded by $\epsilon = 2/255$. In particular, we are able to force zero accuracy when we combine STE with the single-step FGSM attack bounded by $\epsilon = 16/255$. In the case of the iterative PGD attacks, zero accuracy is achieved with ϵ as small as 4. We are not much concerned with the fact that we cannot achieve zero accuracy with the PGD attack bounded by $\epsilon = 2/255$ for two reasons. Firstly, PGD attacks bounded by larger ϵ result in zero accuracy with adversarial perturbations that are also imperceptible to humans, as shown in Figure 1 (and more in Figure A.1). Secondly, we expect to get higher success rates if we combine STE with stronger attack algorithms (e.g. Auto-PGD [14]) or better loss functions (e.g. the hinge loss in CW attacks [8]).

We design the loss function to optimize attacks in the physical world, and hence, the STE-augmented attacks perform worse in the digital domain.

We also examine the loss curves to understand how STE improves optimization of perturbations iteratively in the physical world (c.f. Figure 4). The iteration zero on the X-axis corresponds to the random initialization of perturbations before the twelve optimization steps. The cyan dashed horizontal lines represent the empirical minimum value of cross entropy that links to zero accuracy on the six images. By reading the green dotted curves, we learn that the PGD attacks in the digital domain take no more than two iterations to achieve zero accuracy. However, the orange curves with triangle markers below the dashed threshold confirm that the further improved digital perturbations do not transfer to the physical world, as shown earlier in Table 1. The blue curves with circle markers in the middle ground represent our STE-augmented PGD attacks. We find that it only takes five iterations to produce imperceptible adversarial perturbations bounded by $\epsilon = 16/255$ that degrade the accuracy of the target model to zero. Increasing the step size of $1/255$ can further speed up finding effective perturbations, since FGSM succeeds with one step of size $16/255$.

3.4. Discussion

Even though we are able to produce imperceptible adversarial examples that result in zero accuracy, we recognize that there is a large gap between the power of the digital attack and our physical attack, as shown in the loss curves in Figure 4. We identify two possible reasons behind the phenomenon. Firstly, our printout experiments do not always

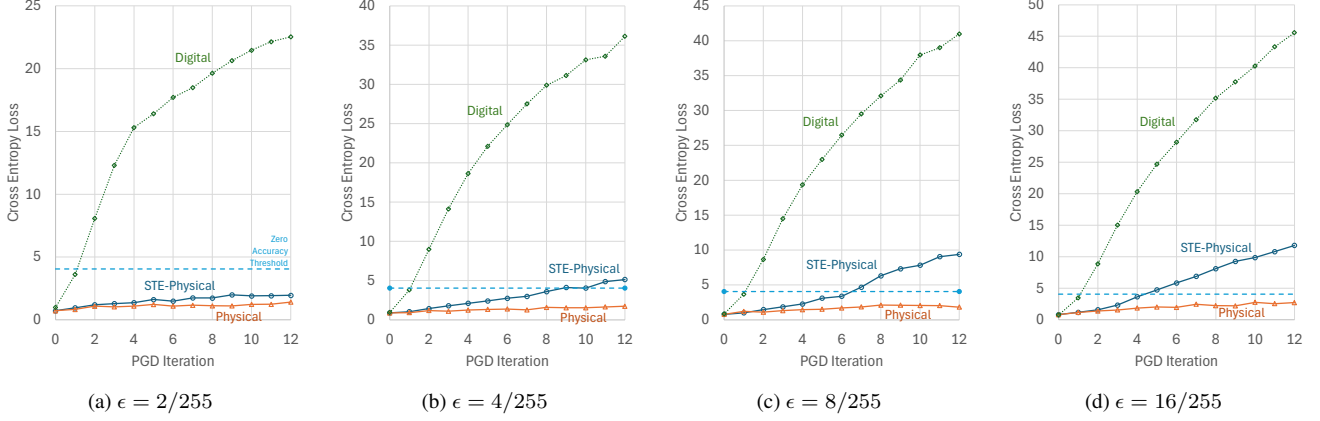


Figure 4. The loss curves of untargeted PGD attacks bounded by four ℓ_∞ norms respectively. PGD in the digital domain (green dotted curve) is always effective in finding adversarial perturbations that increase the cross entropy loss with respect to the ground truth. However, the perturbations are not as effective if we print them out in the physical world (orange curve with triangle markers). STE helps the PGD optimization of adversarial perturbations in the non-differentiable physical environment (blue curve with circle markers). The STE-augmented PGD attack manages to cross the empirical threshold of loss (cyan dashed line) to get 0% accuracy in the physical world with imperceptible adversarial perturbations bounded by ℓ_∞ norms as small as $= 4/255$, as is shown in Figure 1 and Table 1.

perfectly crop out the distorted images from photos (see examples in Figure A.1). Any pixel misalignment would break the assumption of STE, resulting in non-optimal solutions to gradient-sign attacks. Secondly, the image distortions in the physical world constrain the pixel value space, which limits the capability of adversaries in the physical world. Although existing works, including this paper, fail to find a distortion that can defend computer vision models against adversarial examples in the digital domain, researchers may get inspired by the physical distortions in search of adversarial example solutions.

4. Imperceptible patch perturbations

While global perturbation is the most studied threat model in adversarial machine learning, patch perturbations are more realistic in the physical world. In this section, we extend the STE method to work with the patch perturbation threat model, and demonstrate it in the CARLA simulator.

4.1. STE extension with differentiable rendering

We formalize the visual sensing system under the adversarial patch threat model: given a target model $f(\cdot)$ and a camera $c(\cdot)$, an adversary can add an ℓ_∞ -bounded perturbation δ to a patch image x in the digital domain. The adversary must use a printing device $p(\cdot)$ to render the perturbed patch in the physical world, and it cannot change the surrounding environment e . The end-to-end visual sensing system can be expressed as:

$$y = f(c(p(x + \delta), e)), \quad (4)$$

To overcome non-differentiability, we replace the non-differentiable $c(p(x + \delta), e)$ with $c_d(\delta, x, e)$ such that

$c_d(\delta, x, e)$ is differentiable with respect to δ and use gradient-based methods to optimize the perturbation. As is shown in Figure 5, we use a differentiable rendering engine $r(\cdot)$ and a stop-gradient ($\text{sg}[\cdot]$) operation to construct a differentiable imaging pipeline as:

$$\begin{aligned} g_d(\delta, x, e) &= r(x + \delta) + \text{sg}[c(p(x + \delta), e) - r(x + \delta)] \\ &= r(x + \delta) + C \end{aligned} \quad (5)$$

It is important to note that:

1. $g_d(\delta, x, e)$ outputs the same as $c(p(x + \delta), e)$ does in the forward pass, because $r(x + \delta)$ cancels out $-r(x + \delta)$ numerically.
2. $g_d(\delta, x, e)$ is differentiable with respect to δ through differentiable rendering $r(x + \delta)$.
3. The differentiable renderer $r(\cdot)$ ignores the surrounding environment e .
4. The difference between the non-differentiable $c(p(x + \delta), e)$ and differentiable $r(x + \delta)$ is detached as a constant C for modern autograd engines [29] in the backward pass by the $\text{sg}[\cdot]$ operation.

Therefore, we can approximate the derivative of $f(c(p(x + \delta), e))$ at the point $\hat{\delta}$ as:

$$\begin{aligned} \nabla_{\delta} f(c(p(x + \delta), e))|_{\delta=\hat{\delta}} &\approx \nabla_{\delta} f(g_d(\delta, x, e))|_{\delta=\hat{\delta}} \\ &= \nabla_{\delta} f(r(x + \delta) + C)|_{\delta=\hat{\delta}}. \end{aligned} \quad (6)$$

As long as $r(\cdot)$ renders $x + \delta$ at the same location as in $c(p(x + \delta), e)$, we have the property $c(p(x + \delta), e) \approx r(x + \delta)$ for all pixels of the perturbed image $x + \delta$, thus $\nabla_{\delta} c(p(x + \delta), e) \approx \nabla_{\delta} r(x + \delta)$. The adversary does not care whether $g_d(\delta, x, e)$ is differentiable with respect to e , as the adversary has no control over the surrounding environment.

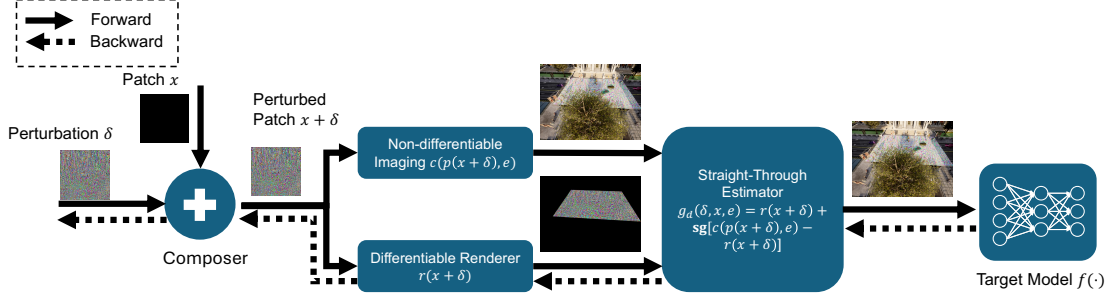


Figure 5. STE combined with differentiable rendering overcomes non-differentiability in the patch threat model.

4.2. Experimental setup

We follow the setup in the DARPA GARD [15] 7th evaluation to evaluate adversarial patches in the CARLA simulator [36]. One big change we introduce in this paper is to render adversarial patches in CARLA for evaluation, while the GARD setup only evaluates the digitally composed patches. The GARD setup allows unbounded adversarial patches, because the patches only take a small portion of the whole scene. In this paper, we also evaluate ℓ_∞ attacks bounded by small ϵ to produce imperceptible adversarial patches.

Dataset: We use a self-collected dataset that is similar to the DARPA GARD 7th evaluation dataset for object detection, which consists of 20 images with green rectangular screens that adversaries can perturb to influence the target model (one in Figure 6, more in Figure A.3). Due to the lack of essential CARLA metadata in the released GARD dataset, we have to recreate the scenes of every image using the OSCAR Datagen Toolkit [13] so that we can render custom textures on the green screens in CARLA. We also use one city art asset (in Figure 6) from CARLA as the starting image to demonstrate imperceptible adversarial perturbations bounded by small ℓ_∞ norms. The rectangular patch can be partially obstructed by other objects (e.g. trees, vehicles).

Target model: We use the Faster R-CNN object detection model provided in Armory [33] as the target model. This model is pre-trained on the MS-COCO dataset [26] and fine-tuned on the CARLA training dataset offered in Armory to detect only two classes: vehicle and pedestrian. The model weights file is publicly available online [37].

Metrics: We report the average precision at IoU threshold of 50% (AP50) as the major performance metric for object detection in the experiments. In addition, we report six TIDE errors to help understand how the model performs in object detection behind the AP50 numbers [5].

Attack: We implement the iterative attacks using the *Modular Adversarial Robustness Toolkit* (MART) [41] framework. Following the parameters of the example attack in ARMORY [36], we use the Adam optimizer to maximize the training loss for 500 iterations with the learning rate $\frac{12.75}{255}$. We use lower learning rates and fewer iterations

for the imperceptible adversarial perturbation experiments. We name the attacks as “[Optimizer]-[Iterations]-[Learning Rate]” in Table 2.

Non-differentiable renderer: CARLA uses UE4 as the renderer which supports complex lighting and materials. The nearby objects and the weather in UE4 also affect the rendering result of the adversarial patch.

Differentiable renderer: Our method does not require a full-function differentiable renderer that is comparable with UE4. Since we only render 2D rectangular patches, we use the *perspective transformation* function in PyTorch [39].

4.3. Results

In Figure 6 we present one example scene out of 20 in CARLA (and more in Figures A.4 to A.13); we render both benign and adversarial patches for comparison. The adversarial patches shown in the three center columns cause many hallucinations to the target object detection model but remain imperceptible.

In Table 2 we report the detailed object detection performance on all 20 images under various attacks. First of all, the model performs similarly (AP50 around 44%) when given three types of benign images: no patch, the patch of a green screen, and the patch of a benign city art painting (Figure 6). Adding ℓ_∞ -bounded perturbations generated by our STE-augmented attacks to the city art painting degrades the object detection performance significantly. The most constrained $\ell_\infty = 2$ attack lowers AP50 from 43.29% to 33.20%. In contrast, the unbounded attack without STE is less powerful than our weakest STE-augmented $\ell_\infty = 2$ attack, which only lowers AP50 to 38.73%. Therefore, we skip the experiments of non-STE attacks with ℓ_∞ bounds.

Our attack with $\ell_\infty = 4$ further lowers AP50 to 17.12%. Subsequently, with $\ell_\infty = 8$, AP50 drops to 4.22%. The TIDE error counts suggest that our attacks introduce many hallucinations (TIDE background errors), and cause many object detection misses (TIDE missed errors). For example, the $\ell_\infty = 8$ attack introduces 95 hallucinations ($15 \rightarrow 110$) and causes 130 objects to vanish ($306 \rightarrow 436$). The unbounded STE-augmented attack completely defeats the tar-

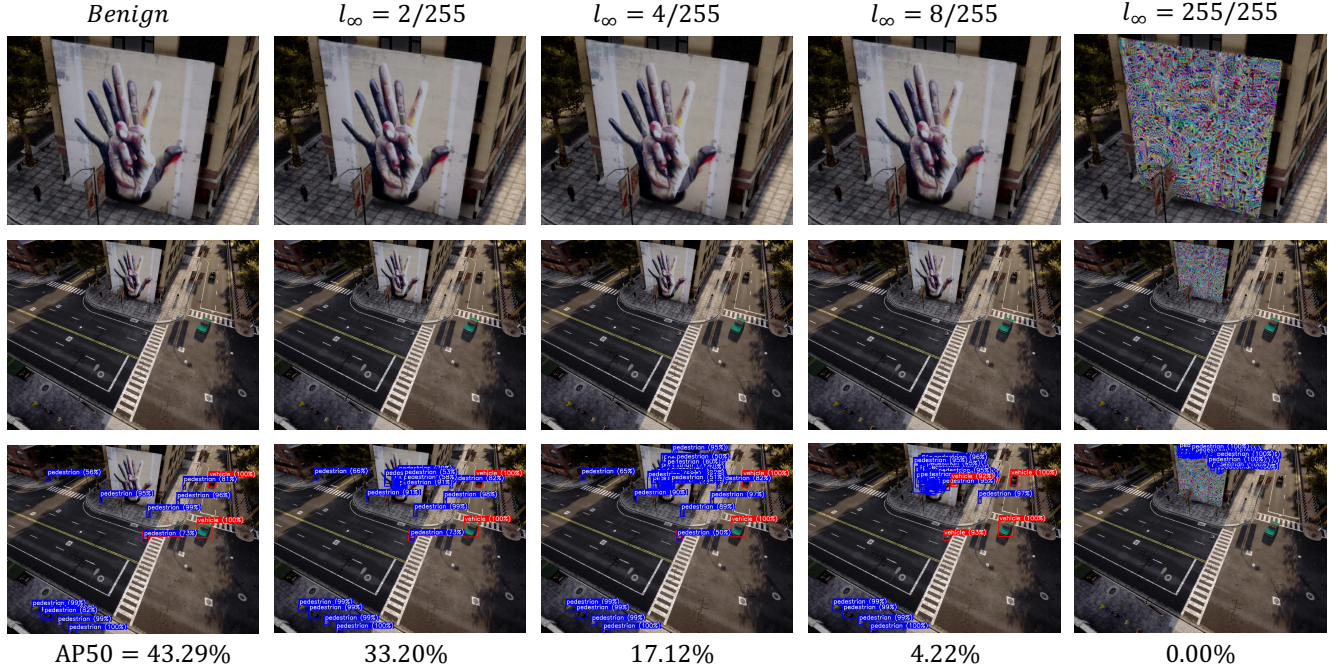


Figure 6. Our method produces imperceptible adversarial examples in CARLA, as the three center columns show. We add the benign images in the left column and the unbounded adversarial examples in the right column for comparison. We also highlight the rectangular patches from the full scenes in the first row, so that it is easier for readers to examine the perturbations.

Adversary Budget	Patch / Attack	STE	TIDE Error Counts						AP50↓
			Class	Box	Other	Dup.	Bg.	Missed	
0 (Benign)	No Patch	-	1	13	1	1	10	303	44.81%
	Green Screen	-	2	10	1	1	10	302	44.74%
	City Art	-	1	9	1	1	15	306	43.29%
$l_\infty = 2$	Adam-200-1	✓	0	16	2	0	44	342	33.20%
$l_\infty = 4$	Adam-200-2	✓	0	20	5	0	86	391	17.12%
$l_\infty = 8$	Adam-200-2	✓	0	19	28	0	110	436	4.22%
Unbounded	Adam-500-12.75	✗	0	19	3	1	16	314	38.73%
	Adam-500-12.75	✓	0	30	13	0	157	476	0.00%

Table 2. STE combined with differentiable rendering produces imperceptible adversarial patches bounded by l_∞ norms in CARLA.

get model (0% AP50) because the highly confident adversarial hallucinations overwhelm the detection of other objects that are less confident.

4.4. Discussion and Future Work

We have demonstrated that combining STE with differentiable rendering produces imperceptible adversarial perturbations to rectangular patches. One natural extension is to produce imperceptible adversarial camouflage for 3D objects in the physical world. Since differentiable renderers that support 3D meshes, such as PyTorch3D [30], are readily available, users should be able to produce imperceptible

adversarial textures using our approach Figure 5. The other interesting direction is to combine with EoT, so that we can make imperceptible adversarial examples in the physical world that are robust to environmental fluctuations.

5. Conclusion

In this work, we show that our STE-augmented attacks against DNN-based visual sensing systems with non-differentiable distortions are effective: 1) they force zero classification accuracy in the global perturbation threat model; 2) cause near zero AP50 (4.22%) in object detection in the patch perturbation threat model. In contrast to

existing physically realizable adversarial examples, our approach produces imperceptible adversarial examples, making it harder to detect them in the physical world. This necessitates further investigation into the efficacy of our method, and its implications for real-world systems. Simultaneously, it will be crucial to evaluate existing defense solutions against such attacks to better understand the landscape of the threat.

Acknowledgments

This work is partially supported by the Defense Advanced Research Projects Agency (DARPA) under Contract No. HR001119S0026.

References

- [1] Anish Athalye, Nicholas Carlini, and David Wagner. Obfuscated gradients give a false sense of security: Circumventing defenses to adversarial examples. In *International conference on machine learning*, pages 274–283. PMLR, 2018. 2, 4
- [2] Anish Athalye, Logan Engstrom, Andrew Ilyas, and Kevin Kwok. Synthesizing robust adversarial examples. In *International conference on machine learning*, pages 284–293. PMLR, 2018. 1, 3
- [3] Farhan A Baqai, J-H Lee, A Ufuk Agar, and Jan P Allebach. Digital color halftoning. *IEEE Signal Processing Magazine*, 22(1):87–96, 2005. 3
- [4] Yoshua Bengio, Nicholas Léonard, and Aaron Courville. Estimating or propagating gradients through stochastic neurons for conditional computation. *arXiv preprint arXiv:1308.3432*, 2013. 3
- [5] Daniel Bolya, Sean Foley, James Hays, and Judy Hoffman. Tide: A general toolbox for identifying object detection errors. In *ECCV*, 2020. 7
- [6] Anneliese Braunegg, Amartya Chakraborty, Michael Krundick, Nicole Lape, Sara Leary, Keith Manville, Elizabeth Merkhofer, Laura Strickhart, and Matthew Walmer. Apricot: A dataset of physical adversarial attacks on object detection. In *Computer Vision–ECCV 2020: 16th European Conference, Glasgow, UK, August 23–28, 2020, Proceedings, Part XXI 16*, pages 35–50. Springer, 2020. 1
- [7] Mark Buckler, Suren Jayasuriya, and Adrian Sampson. Reconfiguring the imaging pipeline for computer vision. In *Proceedings of the IEEE International Conference on Computer Vision*, pages 975–984, 2017. 2, 3
- [8] Nicholas Carlini and David Wagner. Towards evaluating the robustness of neural networks. In *2017 IEEE Symposium on Security and Privacy (SP)*, pages 39–57. Ieee, 2017. 5
- [9] Nicholas Carlini, Anish Athalye, Nicolas Papernot, Wieland Brendel, Jonas Rauber, Dimitris Tsipras, Ian Goodfellow, Aleksander Madry, and Alexey Kurakin. On evaluating adversarial robustness. *arXiv preprint arXiv:1902.06705*, 2019. 2
- [10] Nicholas Carlini, Milad Nasr, Christopher A Choquette-Choo, Matthew Jagielski, Irena Gao, Pang Wei W Koh, Daphne Ippolito, Florian Tramer, and Ludwig Schmidt. Are aligned neural networks adversarially aligned? *Advances in Neural Information Processing Systems*, 36, 2024. 2
- [11] Shang-Tse Chen, Cory Cornelius, Jason Martin, and Duen Horng Chau. Shapeshifter: Robust physical adversarial attack on faster r-cnn object detector. In *Machine Learning and Knowledge Discovery in Databases: European Conference, ECML PKDD 2018, Dublin, Ireland, September 10–14, 2018, Proceedings, Part I 18*, pages 52–68. Springer, 2019. 1, 3
- [12] Jeremy Cohen, Elan Rosenfeld, and Zico Kolter. Certified adversarial robustness via randomized smoothing. In *international conference on machine learning*, pages 1310–1320. PMLR, 2019. 2
- [13] Cory Cornelius, Luis Murillo, and Weilin Xu. Oscar datagen toolkit. <https://github.com/IntelLabs/OSCAR/tree/main/lib/oscar-datagen-toolkit>, 2023. 7
- [14] Francesco Croce and Matthias Hein. Reliable evaluation of adversarial robustness with an ensemble of diverse parameter-free attacks. In *International conference on machine learning*, pages 2206–2216. PMLR, 2020. 5
- [15] DARPA. Guaranteeing AI Robustness Against Deception (GARD). <https://www.darpa.mil/program/guaranteeing-ai-robustness-against-deception>. Accessed: 2024-07-10. 7
- [16] Jia Deng, Wei Dong, Richard Socher, Li-Jia Li, Kai Li, and Li Fei-Fei. Imagenet: A large-scale hierarchical image database. In *2009 IEEE conference on computer vision and pattern recognition*, pages 248–255. Ieee, 2009. 4
- [17] Yao Deng, Tiehua Zhang, Guannan Lou, Xi Zheng, Jiong Jin, and Qing-Long Han. Deep learning-based autonomous driving systems: A survey of attacks and defenses. *IEEE Transactions on Industrial Informatics*, 17(12):7897–7912, 2021. 1
- [18] Alexey Dosovitskiy, German Ros, Felipe Codevilla, Antonio Lopez, and Vladlen Koltun. Carla: An open urban driving simulator. In *Conference on robot learning*, pages 1–16. PMLR, 2017. 2
- [19] Epic Games. Unreal Engine. <https://www.unrealengine.com>. Accessed: 2024-07-10. 2
- [20] Nathan Hamiel. Black Hat AI Track Submissions: Observations and Feedback. <http://web.archive.org/web/20241106221125/https://i.blackhat.com/BH-US-24/BH-AI-Track-Submissions-Nathan-Hamiel.pdf>. Accessed: 2024-11-06. 1
- [21] Steve TK Jan, Joseph Messou, Yen-Chen Lin, Jia-Bin Huang, and Gang Wang. Connecting the digital and physical world: Improving the robustness of adversarial attacks. In *Proceedings of the AAAI Conference on Artificial Intelligence*, pages 962–969, 2019. 1, 3
- [22] Melanie Jutras, Ethan Liang, Sara Leary, Chris Ward, and Keith Manville. Detecting physical adversarial patch attacks with object detectors. In *2022 IEEE Applied Imagery Pattern Recognition Workshop (AIPR)*, pages 1–7. IEEE, 2022. 3
- [23] Hiroharu Kato, Deniz Beker, Mihai Morariu, Takahiro Ando, Toru Matsuoka, Wadim Kehl, and Adrien Gaidon.

- Differentiable rendering: A survey. *arXiv preprint arXiv:2006.12057*, 2020. 3
- [24] Alexey Kurakin, Ian J Goodfellow, and Samy Bengio. Adversarial examples in the physical world. In *Artificial intelligence safety and security*, pages 99–112. Chapman and Hall/CRC, 2018. 3, 4, 5
- [25] Bin Liang, Jiachun Li, and Jianjun Huang. We can always catch you: Detecting adversarial patched objects with or without signature. *arXiv preprint arXiv:2106.05261*, 2021. 3
- [26] Tsung-Yi Lin, Michael Maire, Serge Belongie, James Hays, Pietro Perona, Deva Ramanan, Piotr Dollár, and C Lawrence Zitnick. Microsoft coco: Common objects in context. In *Computer Vision–ECCV 2014: 13th European Conference, Zurich, Switzerland, September 6–12, 2014, Proceedings, Part V 13*, pages 740–755. Springer, 2014. 7
- [27] Aleksander Madry, Aleksandar Makelov, Ludwig Schmidt, Dimitris Tsipras, and Adrian Vladu. Towards deep learning models resistant to adversarial attacks. *arXiv preprint arXiv:1706.06083*, 2017. 1, 2
- [28] Ali Mosleh, Avinash Sharma, Emmanuel Onzon, Fahim Mannan, Nicolas Robidoux, and Felix Heide. Hardware-in-the-loop end-to-end optimization of camera image processing pipelines. In *Proceedings of the IEEE/CVF Conference on Computer Vision and Pattern Recognition*, pages 7529–7538, 2020. 3
- [29] Adam Paszke, Sam Gross, Francisco Massa, Adam Lerer, James Bradbury, Gregory Chanan, Trevor Killeen, Zeming Lin, Natalia Gimelshein, Luca Antiga, et al. Pytorch: An imperative style, high-performance deep learning library. *Advances in neural information processing systems*, 32, 2019. 6
- [30] Nikhila Ravi, Jeremy Reizenstein, David Novotny, Taylor Gordon, Wan-Yen Lo, Justin Johnson, and Georgia Gkioxari. Accelerating 3d deep learning with pytorch3d. *arXiv preprint arXiv:2007.08501*, 2020. 8
- [31] Khosro Rezaee, Sara Mohammad Rezakhani, Mohammad R Khosravi, and Mohammad Kazem Moghimi. A survey on deep learning-based real-time crowd anomaly detection for secure distributed video surveillance. *Personal and Ubiquitous Computing*, 28(1):135–151, 2024. 1
- [32] Mahmood Sharif, Sruti Bhagavatula, Lujo Bauer, and Michael K Reiter. Accessorize to a crime: Real and stealthy attacks on state-of-the-art face recognition. In *Proceedings of the 2016 acm sigsac conference on computer and communications security*, pages 1528–1540, 2016. 3
- [33] David Slater and Lucas Cadalzo. *armory*, 2023. 7
- [34] Naufal Suryanto, Yongsu Kim, Hyoeun Kang, Harashta Tatimma Larasati, Youngyeo Yun, Thi-Thu-Huong Le, Hunmin Yang, Se-Yoon Oh, and Howon Kim. Dta: Physical camouflage attacks using differentiable transformation network. In *Proceedings of the IEEE/CVF Conference on Computer Vision and Pattern Recognition*, pages 15305–15314, 2022. 3
- [35] Christian Szegedy, Wojciech Zaremba, Ilya Sutskever, Joan Bruna, Dumitru Erhan, Ian Goodfellow, and Rob Fergus. Intriguing properties of neural networks. *arXiv preprint arXiv:1312.6199*, 2013. 1
- [36] ARMORY Team. Adversarial Patch Attack against CARLA Object Detection. https://github.com/twosixlabs/armory/blob/v0.19.2/scenario_configs/eval7/carla_overhead_object_detection/carla_obj_det_adversarialpatch_targeted_undefended.json, . Accessed: 2024-02-02. 7
- [37] ARMORY Team. CARLA Object Detection Model Weights for GARD Eval7. https://armory-public-data.s3.amazonaws.com/model-weights/carla_rgb_weights_eval7and8.pt, . Accessed: 2024-02-02. 7
- [38] OpenCV Team. Detection of ArUco Markers. https://docs.opencv.org/4.x/d5/dae/tutorial_aruco_detection.html, . Accessed: 2024-11-11. 4
- [39] PyTorch Team. PyTorch Perspective Transformation API. <https://pytorch.org/vision/main/generated/torchvision.transforms.functional.perspective.html>, . Accessed: 2024-02-02. 7
- [40] Zuxuan Wu, Ser-Nam Lim, Larry S Davis, and Tom Goldstein. Making an invisibility cloak: Real world adversarial attacks on object detectors. In *Computer Vision–ECCV 2020: 16th European Conference, Glasgow, UK, August 23–28, 2020, Proceedings, Part IV 16*, pages 1–17. Springer, 2020. 1
- [41] Weilin Xu, Cory Cornelius, and Luis Murillo. Modular adversarial robustness toolkit. <https://github.com/IntelLabs/MART>, 2023. 7
- [42] Jiawei Zhou, Linye Lyu, Daojing He, and Yu Li. Rauca: A novel physical adversarial attack on vehicle detectors via robust and accurate camouflage generation. *arXiv preprint arXiv:2402.15853*, 2024. 3

A. Appendix

	0	2	4	8	16
lorikeet					
	lorikeet 99.26%	coucal 80.91%	coucal 99.98%	coucal 100.00%	coucal 100.00%
Eskimo dog					
	Eskimo dog 63.76%	malamute 39.63%	malamute 96.05%	timber wolf 78.39%	malamute 99.97%
puffer					
	puffer 100.00%	puffer 98.44%	electric ray 76.13%	electric ray 99.63%	electric ray 99.85%
ladle					
	hot pot 44.40%	hot pot 72.35%	Petri dish 58.79%	potter's wheel 97.75%	potter's wheel 99.81%
piggy bank					
	piggy bank 99.55%	piggy bank 88.46%	hog 44.38%	hog 73.50%	hog 79.16%
hot pot					
	hot pot 47.80%	caldron 97.01%	caldron 99.74%	caldron 99.92%	caldron 99.98%

Figure A.1. Results of the 12-step PGD attack combined with STE on photos of printouts. We annotate the ground truth on the left, and the ℓ_∞ bounds at the top. The prediction of the target ResNet50 model is presented below the image. The white edges (most obvious in the “piggy bank” row) are the result of imperfect cropping of the photos.

	0	2	4	8	16
lorikeet	 lorikeet 99.26%	 lorikeet 87.19%	 indigo bunting 45.59%	 indigo bunting 57.13%	 indigo bunting 87.54%
Eskimo dog	 Eskimo dog 63.76%	 Eskimo dog 51.37%	 Siberian husky 43.66%	 Siberian husky 45.27%	 timber wolf 64.94%
puffer	 puffer 100.00%	 puffer 99.91%	 puffer 96.86%	 puffer 60.23%	 electric ray 95.35%
ladle	 hot pot 44.40%	 hot pot 40.77%	 hot pot 37.87%	 potter's wheel 25.32%	 potter's wheel 16.46%
piggy bank	 piggy bank 99.55%	 piggy bank 91.83%	 piggy bank 63.58%	 hog 45.99%	 hog 20.60%
hot pot	 hot pot 47.80%	 caldron 73.93%	 caldron 91.76%	 caldron 95.97%	 caldron 29.86%

Figure A.2. Results of the FGSM attack combined with STE on photos of printouts. We annotate the ground truth on the left, and the ℓ_∞ bounds at the top. The prediction of the target ResNet50 model is presented below the image. The white edges (most obvious in the “piggy bank” row) are the result of imperfect cropping of the photos.

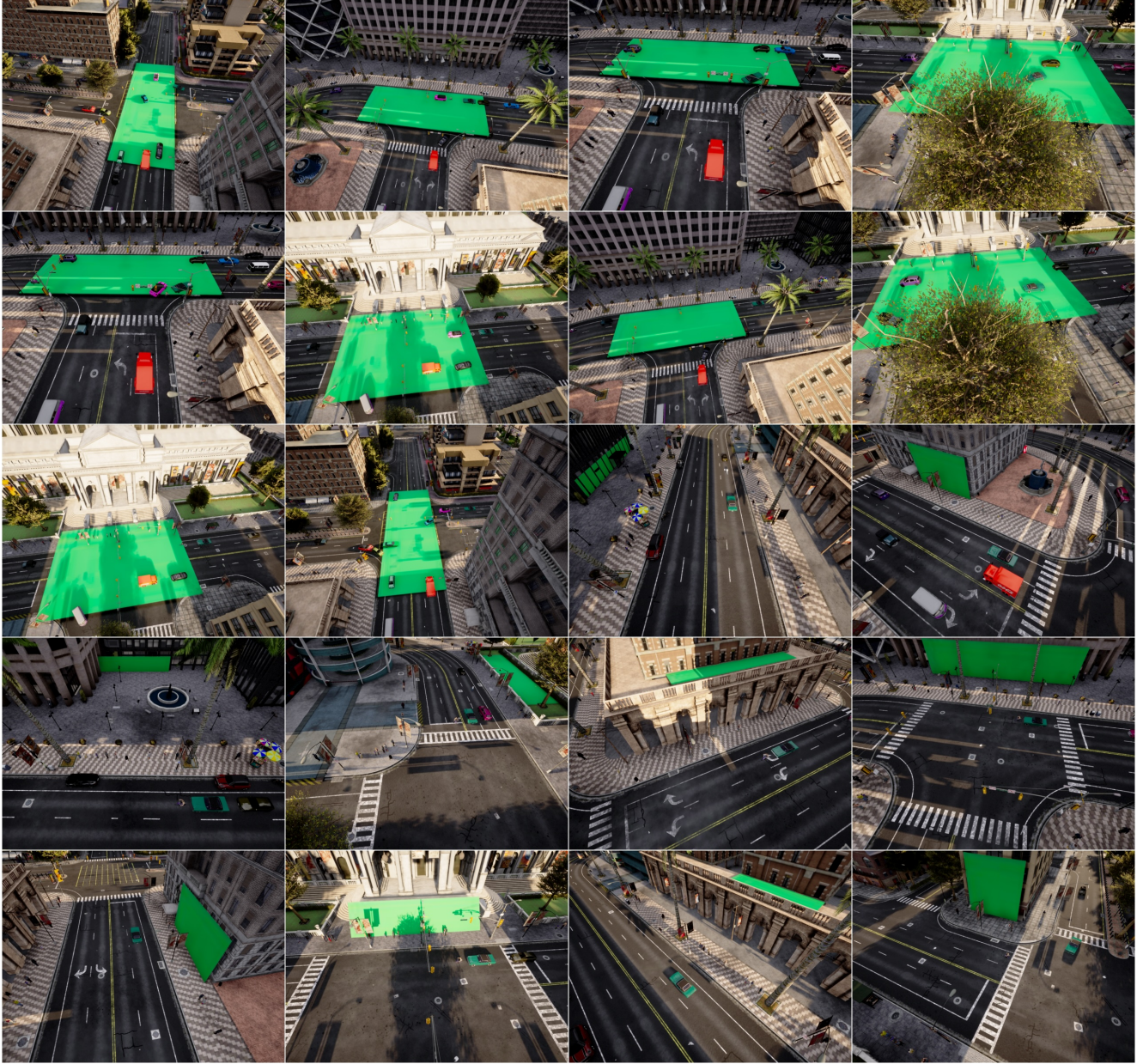


Figure A.3. We recreated the scenes of all 20 images of the DARPA GARD 7th evaluation dataset for object detection in order to render adversarial patches on the green screens in CARLA. We use the bottom right scene to demonstrate imperceptible adversarial patches in the paper.

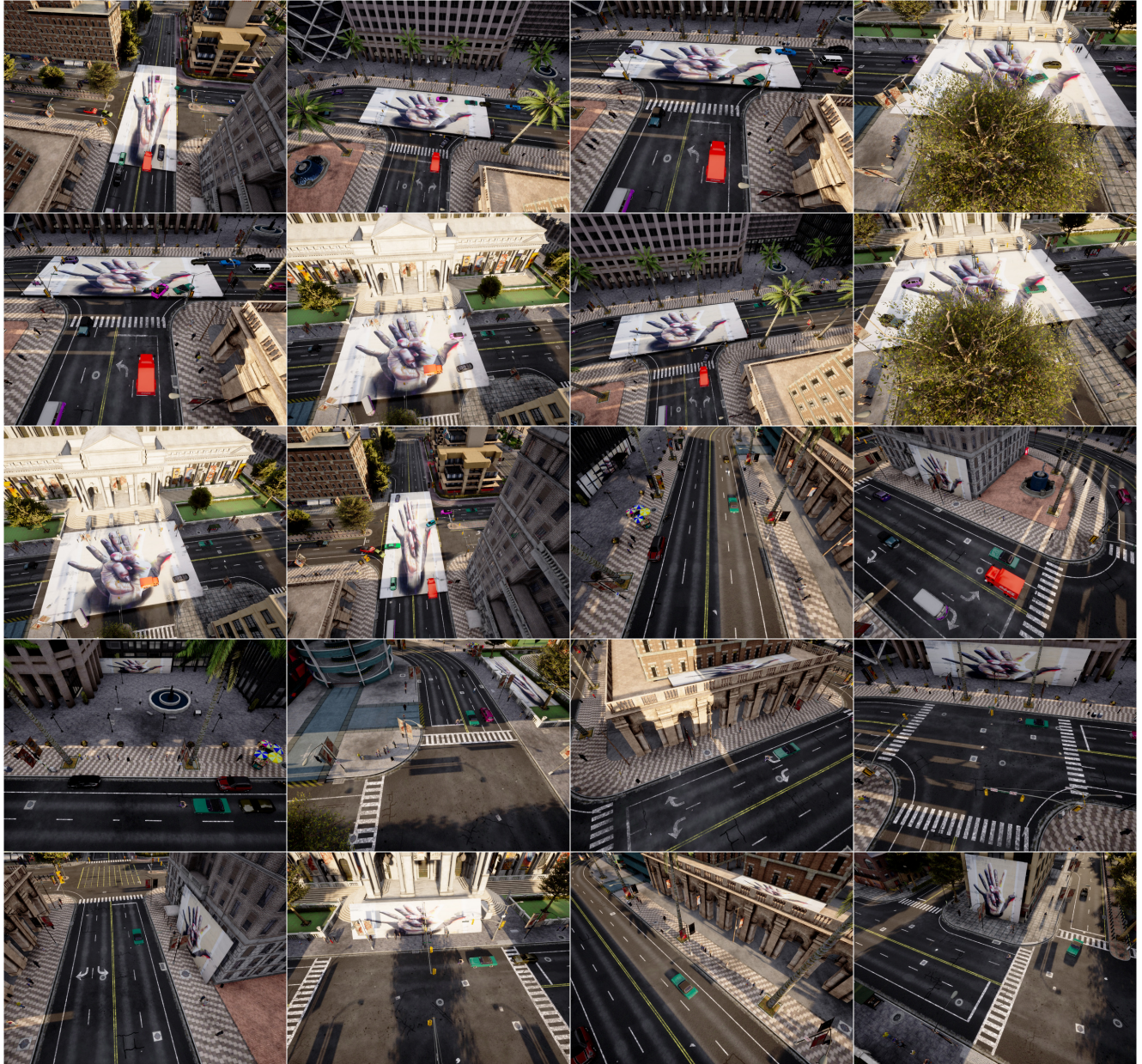


Figure A.4. Rendering the benign city art patch in CARLA.



Figure A.5. Predictions of the target Faster R-CNN model in CARLA, with the benign city art patch.

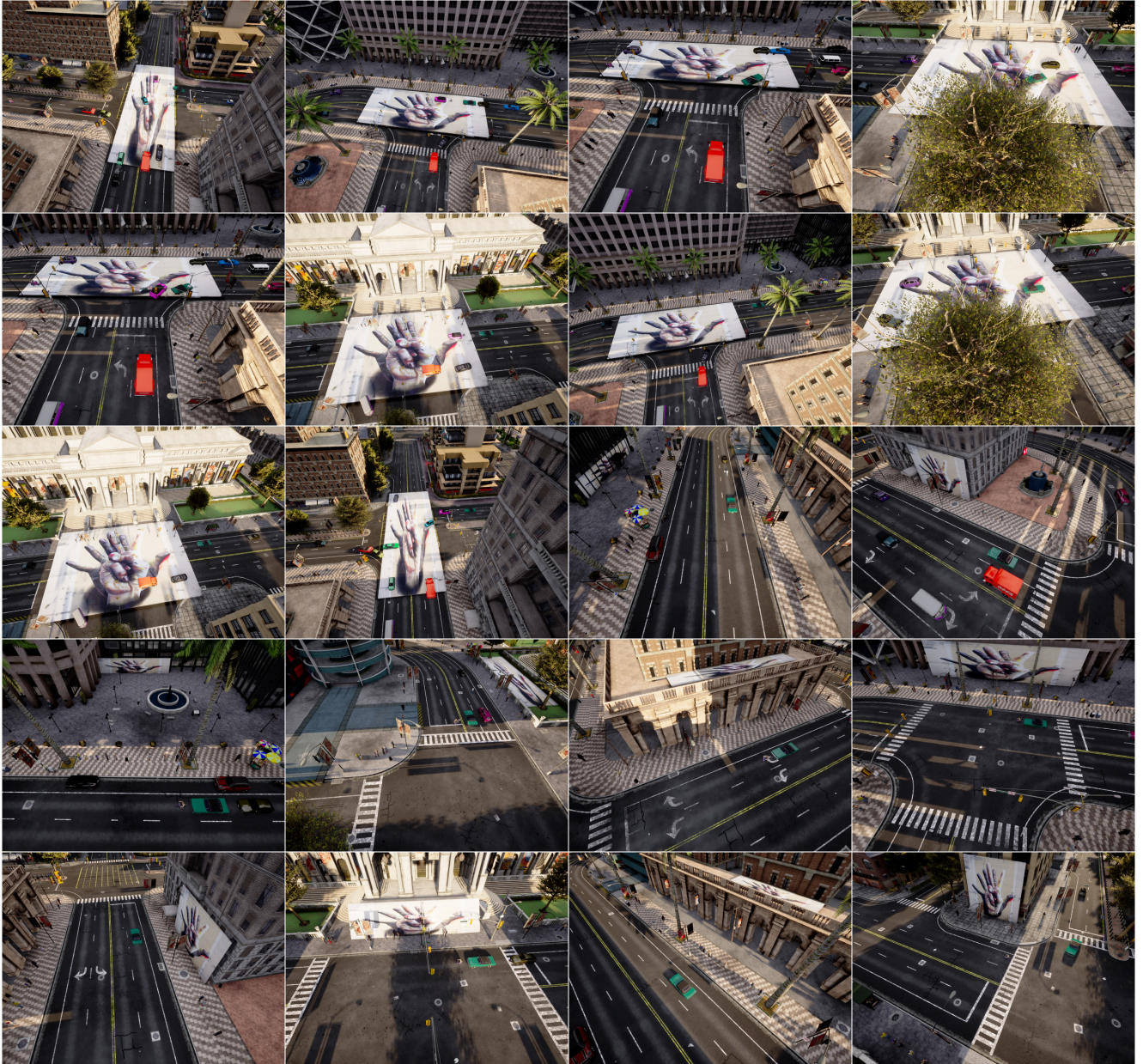


Figure A.6. Rendering adversarial patches generated by the STE-augmented attack bounded by $\ell_\infty = 2$ in CARLA.

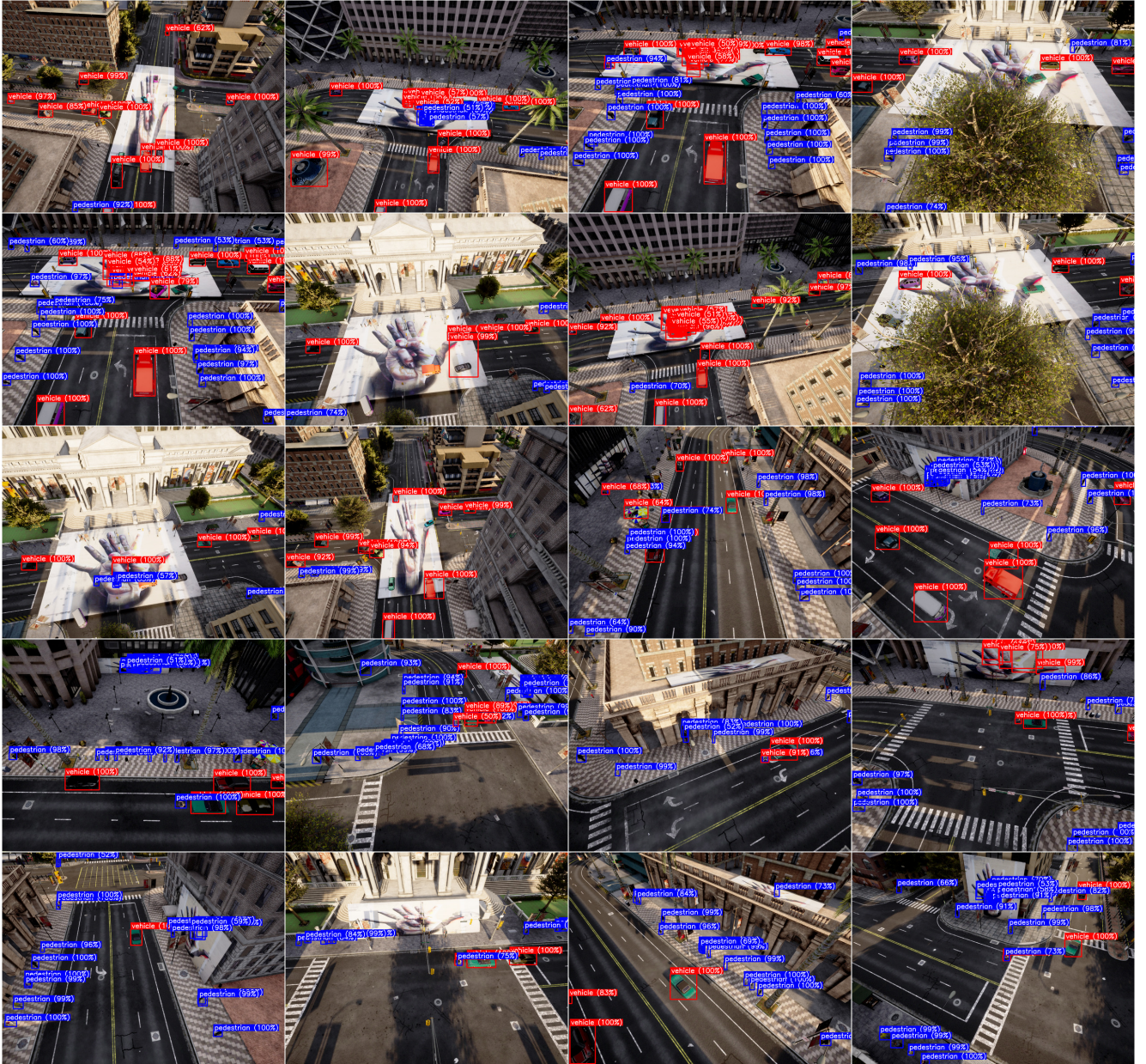


Figure A.7. Predictions of the target model in CARLA, with adversarial patches generated by the $\ell_\infty = 2$ STE-augmented attack.

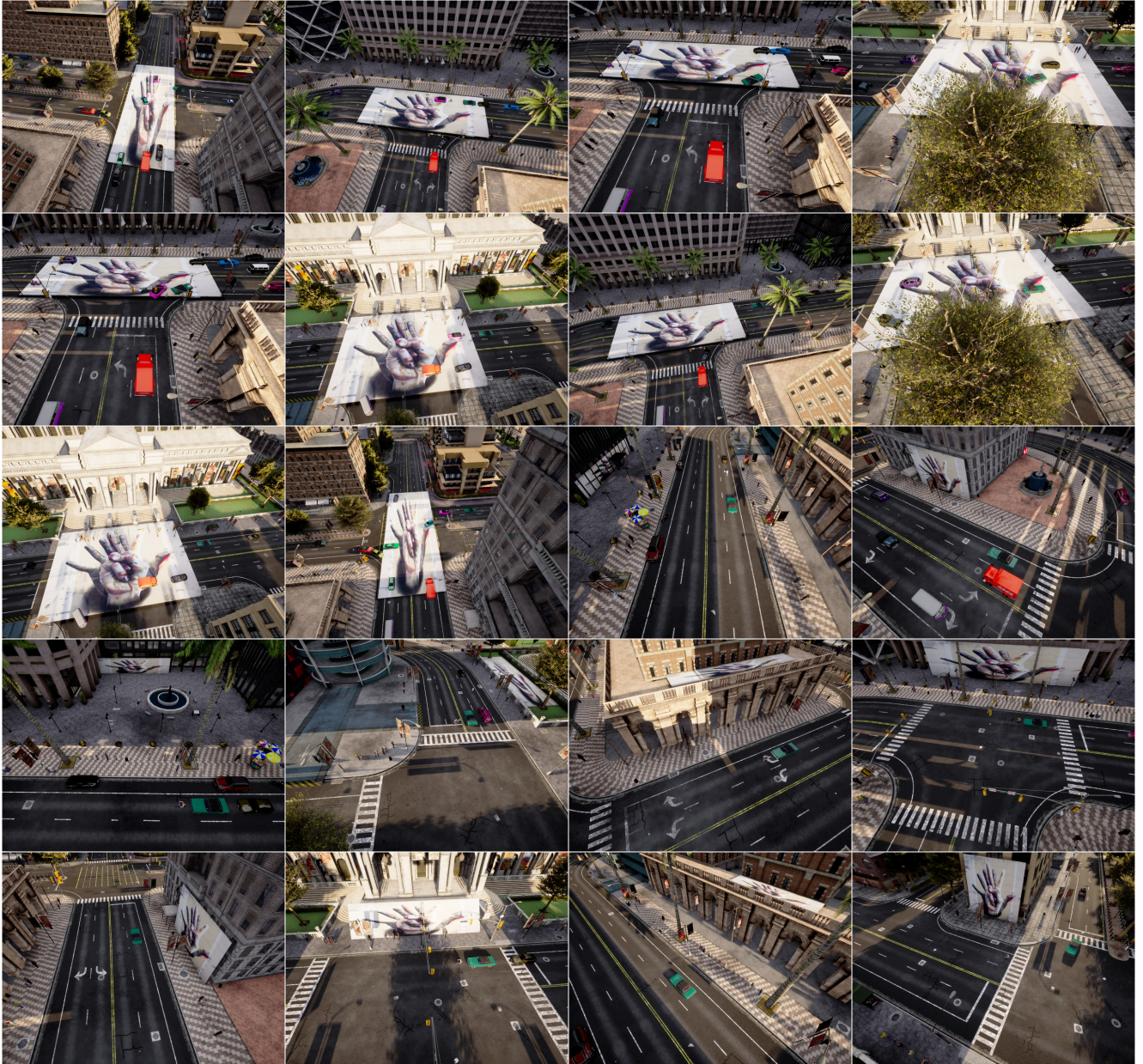


Figure A.8. Rendering adversarial patches generated by the STE-augmented attack bounded by $\ell_\infty = 4$ in CARLA.

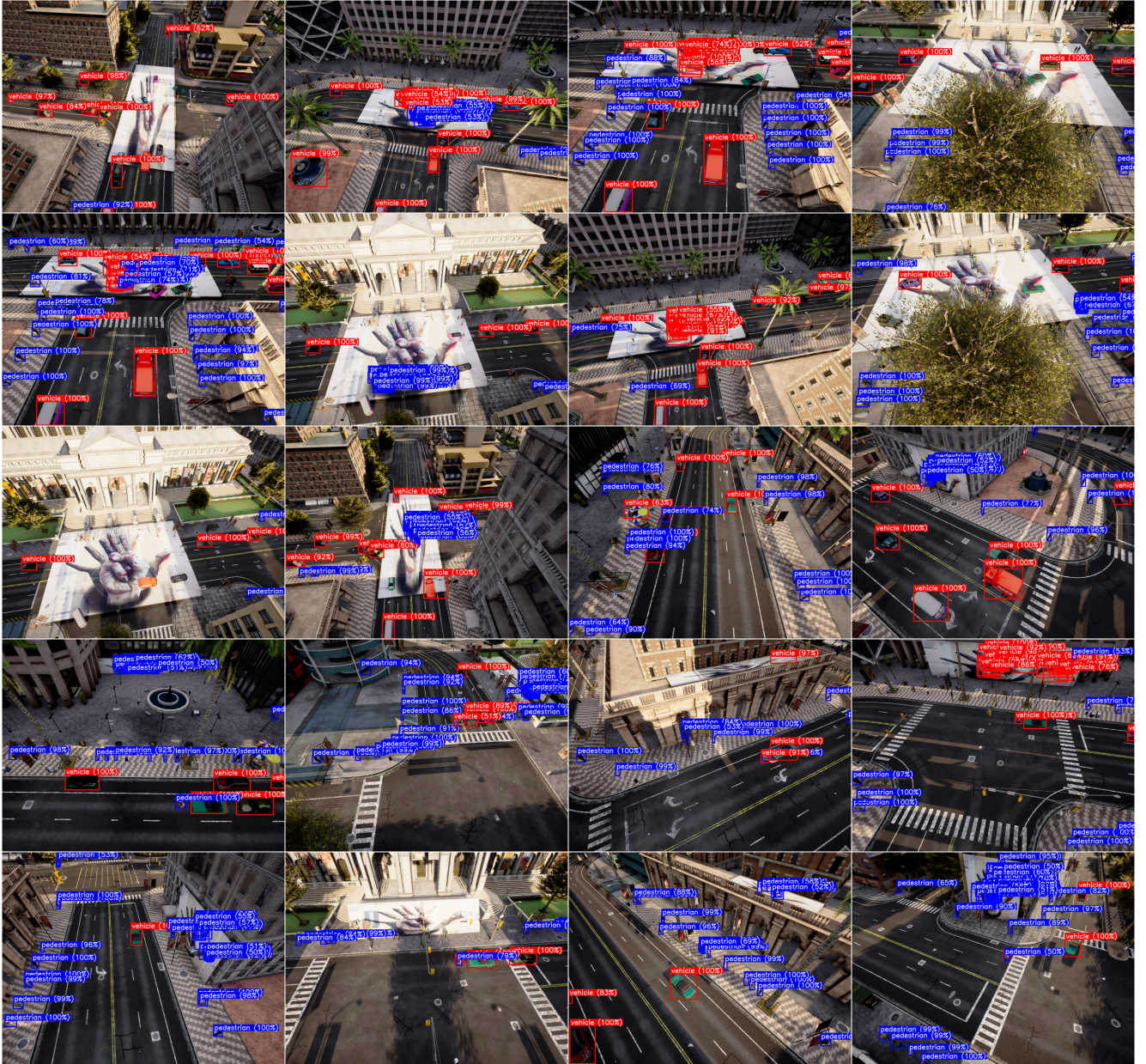


Figure A.9. Predictions of the target model in CARLA, with adversarial patches generated by the $\ell_\infty = 4$ STE-augmented attack.



Figure A.10. Rendering adversarial patches generated by the STE-augmented attack bounded by $\ell_\infty = 8$ in CARLA.

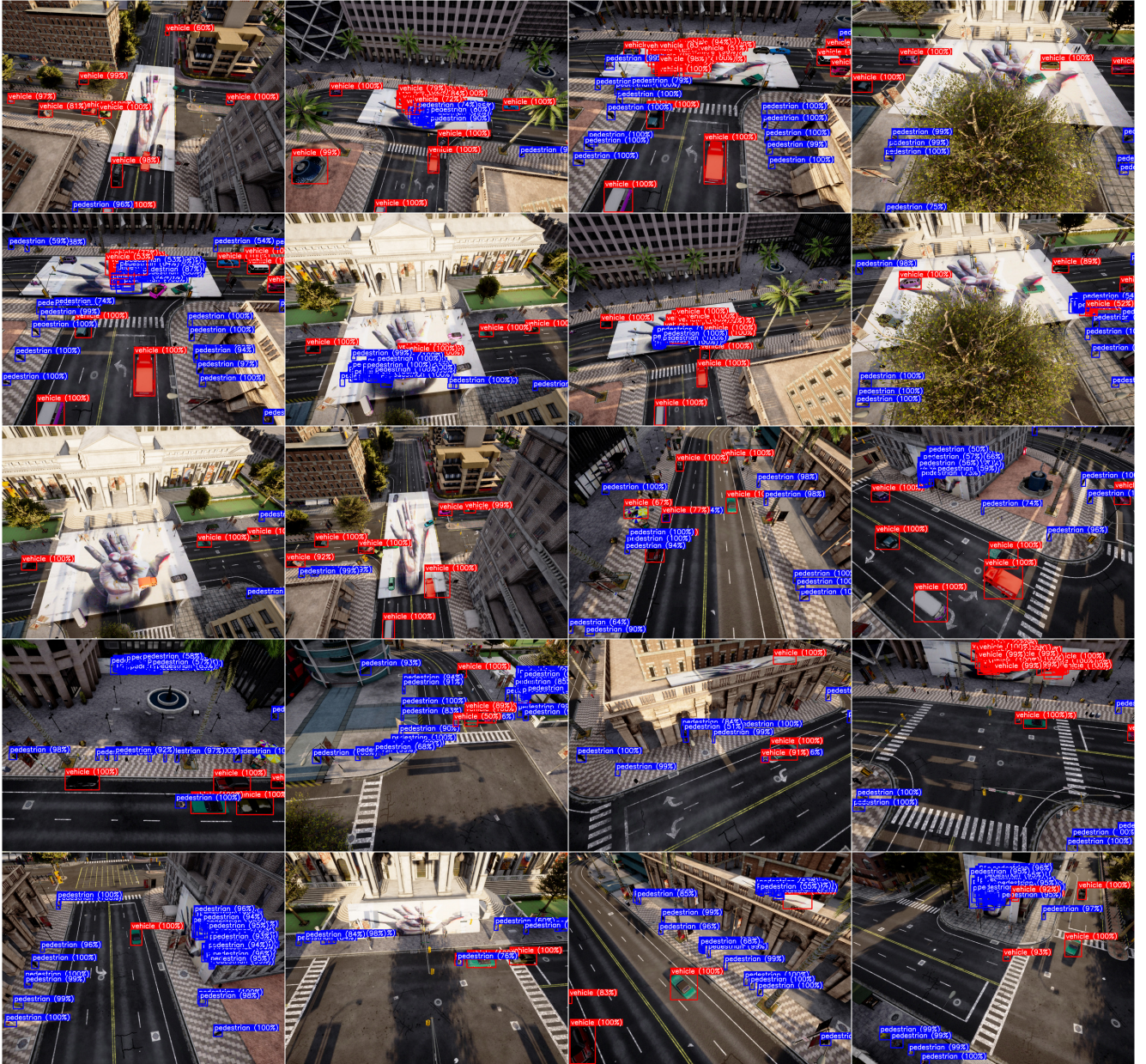


Figure A.11. Predictions of the target model in CARLA, with adversarial patches generated by the $\ell_\infty = 8$ STE-augmented attack.



Figure A.12. Rendering adversarial patches generated by the unbounded STE-augmented attack in CARLA.

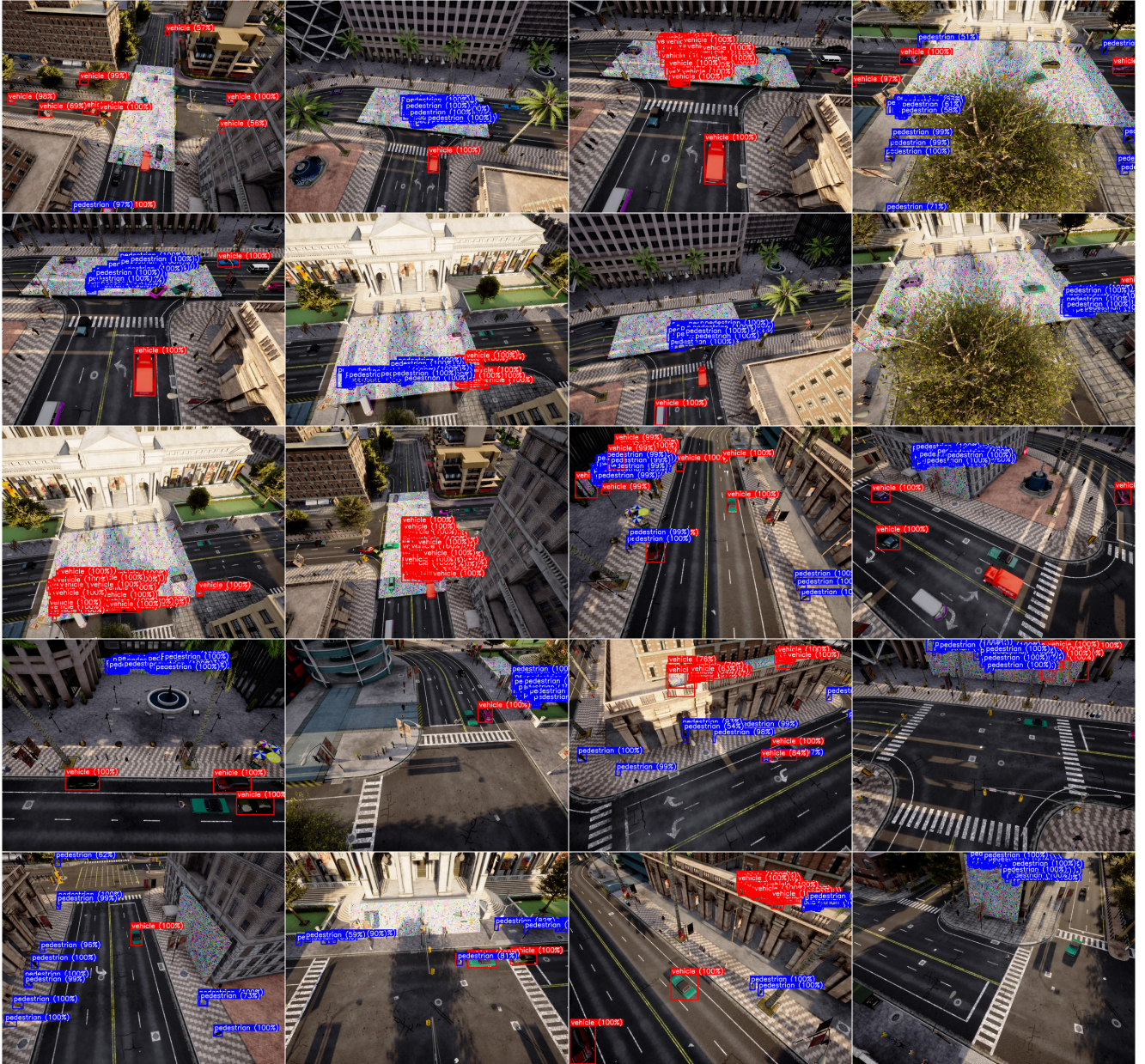


Figure A.13. Predictions of the target model in CARLA, with unbounded adversarial patches generated by the STE-augmented attack.